ELSEVIER

Ceramics International 30 (2004) 635–641

CERAMICS INTERNATIONAL

www.elsevier.com/locate/ceramint

Fracture toughness of hot-pressed $Lu_2Si_2O_7$–Si_3N_4 and $Lu_4Si_2O_7N_2$–Si_3N_4 ceramics and correlation to microstructure and grain-boundary phases

Shuqi Guo*, Naoto Hirosaki, Yoshinobu Yamamoto, Toshiyuki Nishimura, Mamoru Mitomo

Advanced Materials Laboratory, National Institute for Materials Science, 1-1 Namiki, Tsukuba, Ibaraki 305-0044, Japan

Received 22 May 2003; received in revised form 15 June 2003; accepted 11 July 2003

Available online 18 March 2004

Abstract

$Lu_2Si_2O_7$–Si_3N_4 and $Lu_4Si_2O_7N_2$–Si_3N_4 composition ceramics were hot-pressed sintered. Microstructure was characterized by using scanning electron microscope and quantitative image analysis. The $Lu_2Si_2O_7$–Si_3N_4 composition showed a fine-grained microstructure with average grain diameter size of 0.27 μm, whereas the grains of $Lu_4Si_2O_7N_2$–Si_3N_4 composition were coarser with an average grain diameter of 0.48 μm. On the other hand, fracture toughness of the two compositions was evaluated by means of Vickers indentation crack size measurements. Fracture toughness of $Lu_4Si_2O_7N_2$–Si_3N_4 composition was greater than that of $Lu_2Si_2O_7$–Si_3N_4 composition. The greater fracture toughness for $Lu_4Si_2O_7N_2$–Si_3N_4 composition was predominantly caused by increase in grain size and volume fraction of needle-like Si_3N_4 grains compared with $Lu_2Si_2O_7$–Si_3N_4 composition.

Keywords: B. Grain size; B. Grain boundary; C. Fracture; D. Si_3N_4; Lu_2O_3 additive

1. Introduction

A new type of silicon nitride (Si_3N_4) ceramic sintered with Lu_2O_3 additive developed recently has shown significant improvements in the high-temperature properties, including strength, creep resistance, and resistance to oxidation, compared with the existing Si_3N_4 ceramics with other additives (e.g. MgO, Al_2O_3, Sm_2O_3, Er_2O_3, Y_2O_3, Yb_2O_3, etc.) [1–8]. The most noticeable properties of the Lu_2O_3-doped Si_3N_4 ceramic are its excellent creep resistance and oxidation resistance at high temperatures [7,8], which have never been achieved by the Si_3N_4 ceramics with other additives [2–4]. This has made further development and study of the Si_3N_4 ceramics with Lu_2O_3 additives an important topic of interest.

On the other hand, one of the major limitation for assuring the reliability and lifetime of such ceramic materials is their relatively low fracture toughness/resistance [9,10]. Studies have been reported that the fracture toughness was considerably improved when the sintered Si_3N_4 ceramic material was formed a composite-like microstructure, i.e. large elongated β-Si_3N_4 grains were embedded in a fine-grained β-Si_3N_4 microstructure [11–14]. The toughening mechanisms include crack deflection, grain pullout, elastic bridging, and frictional grain bridging [11–14]. Furthermore, their contribution to increase fracture toughness of Si_3N_4 ceramics is not the same, depending on microstructure, grain diameter size/distribution, and intergranular phase and test environments. For example, the crack deflection is favored above the glass transition temperature of the amorphous grain-boundary phase and larger diameter grains, the grain pullout is favored for smaller diameter grains and/or high temperature; conversely the elastic bridging is favored for larger diameter grains, while the frictional grain bridging mechanism is operated only when crack deflection and grain pullout occur. Although the advantages of the new type of ceramic material in high-temperature oxidizing environments have recently been reported [5–8], its fracture toughness/resistance and correlation to microstructure and grain-boundary phase are little known. Therefore, data are required on fracture toughness for this material and the effects of microstructure and grain-boundary phase need to be understood.

* Corresponding author. Present address: Kagawa Laboratory, Institute of Industrial Science, The University of Tokyo, 4-6-1 Komaba, Meguro-ku, Tokyo 153-8505, Japan. Tel.: +81-3-5452-6328; fax: +81-3-5452-6329.
E-mail address: guo@iis.u-tokyo.ac.jp (S. Guo).

0272-8842/$30.00
doi:10.1016/j.ceramint.2003.07.010

In the present study, three series of Si_3N_4 compositions containing Lu_2O_3 additive were fabricated. Microstructure was characterized using scanning electron microscope (SEM) and grain diameter was quantitatively analyzed. Fracture toughness was estimated by means of Vickers indentation crack size measurements, and correlation to the microstructure and the grain-boundary phases is discussed.

2. Experimental procedure

2.1. Material fabrication

Three series of Si_3N_4 compositions were investigated, one in which the molar ratios of oxides correspond to $Lu_2Si_2O_7$ (SiO_2:Lu_2O_3 = 2:1), and other two in which they correspond to $Lu_4Si_2O_7N_2$ (SiO_2:Lu_2O_3 = 1:4). The two $Lu_4Si_2O_7N_2$–Si_3N_4 compositions were prepared to evaluate effect of amount of Lu_2O_3 on fracture toughness. The detailed compositions of the present materials are shown in Table 1. The starting powders were α-rich Si_3N_4 (SN-E10, UBE Industries, Tokyo, Japan), SiO_2 (99.9% purity, High Purity Chemicals Co., Ltd., Saitama, Japan), Lu_2O_3 (99.9% purity, Shinetsu Chemical Co., Ltd., Tokyo, Japan). A mixture of Lu_2O_3 and SiO_2 was added to Si_3N_4, and then the powder batches were mixed in ethanol for 2 h using a Si_3N_4 ball mill, and subsequently dried in a rotation evaporator. The dried powder was die-pressed into a rectangular-shaped samples, 80 mm × 45 mm × 13 mm, at room temperature under 20 MPa. The samples were placed in a BN-coated graphite die and sintered for 1 h at 1950 °C under a pressure of 20 MPa, in a dry N_2 atmosphere of ∼1 MPa, using a gas pressure sintering furnace (FVPHR-R-10, FRET-40, Fuji Electric Co., Ltd., Tokyo, Japan). Based on results obtained during processing of Si_3N_4 in the Si_3N_4–SiO_2–Yb_2O_3 and Si_3N_4–Lu_2O_3 systems [5,15], the following sintering schedule was chosen:

(1) The samples were heated to 800 °C at 20 °C/min under a 1×10^{-3} Torr vacuum.
(2) At 800 °C a dry N_2 atmosphere flowed through the furnace in which the pressure of N_2 atmosphere maintained at level of 0.925 MPa.
(3) The samples were then heated to 1200 °C at 20 °C/min and subsequently to the final sintered temperature of 1950 °C at 10 °C/min, and were hot-pressed at 1950 °C for 1 h under a pressure of 20 MPa.
(4) Following densification, the samples were cooled in the furnace to room temperature within 2 h.

The density, ρ, of the sintered Si_3N_4 was evaluated by the Archimedes method. The elastic moduli of the hot-pressed Si_3N_4 were determined using ultrasonic equipment. The details of the measurement were reported elsewhere [16,17]. The densities, ρ, Young's modulus, E, shear modulus, G, and Poisson's ratio, ν, for each sintered ceramic are also summarized in Table 1. X-ray diffraction of as-received Si_3N_4 materials exhibited the presence of a major crystalline β-Si_3N_4 phase, together with major $Lu_2Si_2O_7$ secondary phases for $Lu_2Si_2O_7$–Si_3N_4 composition and $Lu_4Si_2O_7N_2$ for $Lu_4Si_2O_7N_2$–Si_3N_4 composition. Transmission electron microscope (TEM) observations confirmed a thin residual amorphous film at two-grain boundaries for the studied materials [18]. In addition, completely crystallized triple grain-junction pockets were observed for the $Lu_2Si_2O_7$–Si_3N_4 composition but for the $Lu_4Si_2O_7N_2$–Si_3N_4 composition these pockets were partially crystallized [18]. Hereafter, three hot-pressed sintered Si_3N_4 ceramics are denoted as $Lu_2Si_2O_7$–Si_3N_4, $Lu_4Si_2O_7N_2$–Si_3N_4(S), and $Lu_4Si_2O_7N_2$–Si_3N_4(L), respectively.

2.2. Microstructure observation and quantitative analysis

The hot-pressed Si_3N_4 materials were cut, and the cut surface was polished with a diamond paste up to 0.5 μm, and the surface of the polished specimens was etched by a CF_4 plasma containing 7.8% O_2. The morphology of the Si_3N_4 microstructure was observed by SEM. These micrographs were then used for quantitative analysis using an image processing system (LUZEX III, Nireko Co., Ltd., Tokyo, Japan). Minimums of 600 grains were analyzed for each material.

2.3. Fracture toughness evaluation

The fracture toughness, K_{IC}, of hot-pressed Si_3N_4 ceramics was determined using Vickers indentation crack size measurements of polished surface. The indentation tests were performed on the polished surface of the specimens by loading with a Vickers indenter (AVK-A, Akashi, Co., Ltd.,

Table 1
Compositions, densities, Young modulus, shear modulus, and Poisson's ratio of the hot-pressed Si_3N_4 ceramics with Lu_2O_3 additives

Material	Compositions (mol%)			Density		Young's modulus E (GPa)	Shear modulus G (GPa)	Poisson's ratio ν
	Si_3N_4	SiO_2	Lu_2O_3	g/m^3	% total density			
$Lu_2Si_2O_7$–Si_3N_4	94	4	2	3.29	100	329	130	0.27
$Lu_4Si_2O_7N_2$–Si_3N_4(S)	94	1.2	4.8	3.47	100	334	131	0.27
$Lu_4Si_2O_7N_2$–Si_3N_4(L)	85	3	12	3.88	100	322	126	0.27

Yokohama, Japan) for 20 s in air at room temperature. The corresponding diagonal of the indentation and crack sizes were measured using an optical microscope attached to the indenter. Three indentation loads of 98, 196, and 294 N were used, and five indents were made at each indentation load.

The fracture toughness, K_{IC}, was calculated using the following relation [19]:

$$K_{IC} = 0.016 \left(\frac{E}{H_v}\right)^{1/2} \left(\frac{P}{c^{3/2}}\right), \quad (1)$$

where E is the Young's modulus (GPa), H_v is the hardness (GPa), P is the indentation load (N), and c is the crack length (μm). The hardness, H_v, was calculated from,

$$H_v = 1854.4 \left(\frac{P}{b^2}\right), \quad (2)$$

where b is the diagonal of the indentation (μm). The crack propagation behavior was observed using SEM.

3. Results

3.1. Microstructural characterization

Fig. 1 shows SEM micrographs of the typical microstructure of the hot-pressed Si_3N_4 ceramics with Lu_2O_3 additives. The general microstructures of the three compositions are similar in morphology. They showed a fine-grained microstructure in which large needle-like β-Si_3N_4 grains were embedded. The formation of large needle-like β-Si_3N_4 grains is attributed to abnormal grain growth as a consequence of local inhomogeneity in the distribution of liquid phase [20]. In the $Lu_2Si_2O_7$–Si_3N_4, a number of the fine grains were observed and the average Si_3N_4 grain size was 0.27 μm in diameter. In both the $Lu_4Si_2O_7N_2$–Si_3N_4(S) and the $Lu_4Si_2O_7N_2$–Si_3N_4(L), however, the Si_3N_4 grains were coarser compared with the $Lu_2Si_2O_7$–Si_3N_4, and their average diameters were 0.48 and 0.49 μm, respectively.

The grain diameter distributions and the aspect ratio distributions of the hot-pressed Lu_2O_3-containing Si_3N_4 ceramics are shown in Fig. 2. The $Lu_2Si_2O_7$–Si_3N_4 is distinct from the $Lu_4Si_2O_7N_2$–Si_3N_4 in the grain diameter distributions. The $Lu_2Si_2O_7$–Si_3N_4 showed a broad grain diameter size distribution (Fig. 2a). On the contrary, the $Lu_4Si_2O_7N_2$–Si_3N_4(S) and $Lu_4Si_2O_7N_2$–Si_3N_4(L) exhibited a bimodal grain diameter size distribution (Fig. 2b and c). However, the bimodal aspect ratio distribution is not observed for the three compositions (Fig. 2d–f). Although the average aspect ratio of the $Lu_2Si_2O_7$–Si_3N_4 is larger than that of the $Lu_4Si_2O_7N_2$–Si_3N_4, the aspect ratio of $Lu_4Si_2O_7N_2$–Si_3N_4(L) is nearly the same as that of $Lu_4Si_2O_7N_2$–Si_3N_4(S) (Table 2). In addition, the volume fraction of large needle-like grains with the aspect ratio $l/d > 4$ and length $l > 2$ μm, which has been confirmed having a significant effect on fracture toughness [11], was also determined during the procedure of quantitative analysis of microstructure for each material. The obtained results are followed as: 1.7% for the $Lu_2Si_2O_7$–Si_3N_4, 2.3% for the $Lu_4Si_2O_7N_2$–Si_3N_4(S), and 3.3% for the $Lu_4Si_2O_7N_2$–Si_3N_4(L). This indicated that volume fraction of needle-like β-Si_3N_4 grains depended strongly on both the grain boundary and amount of additive.

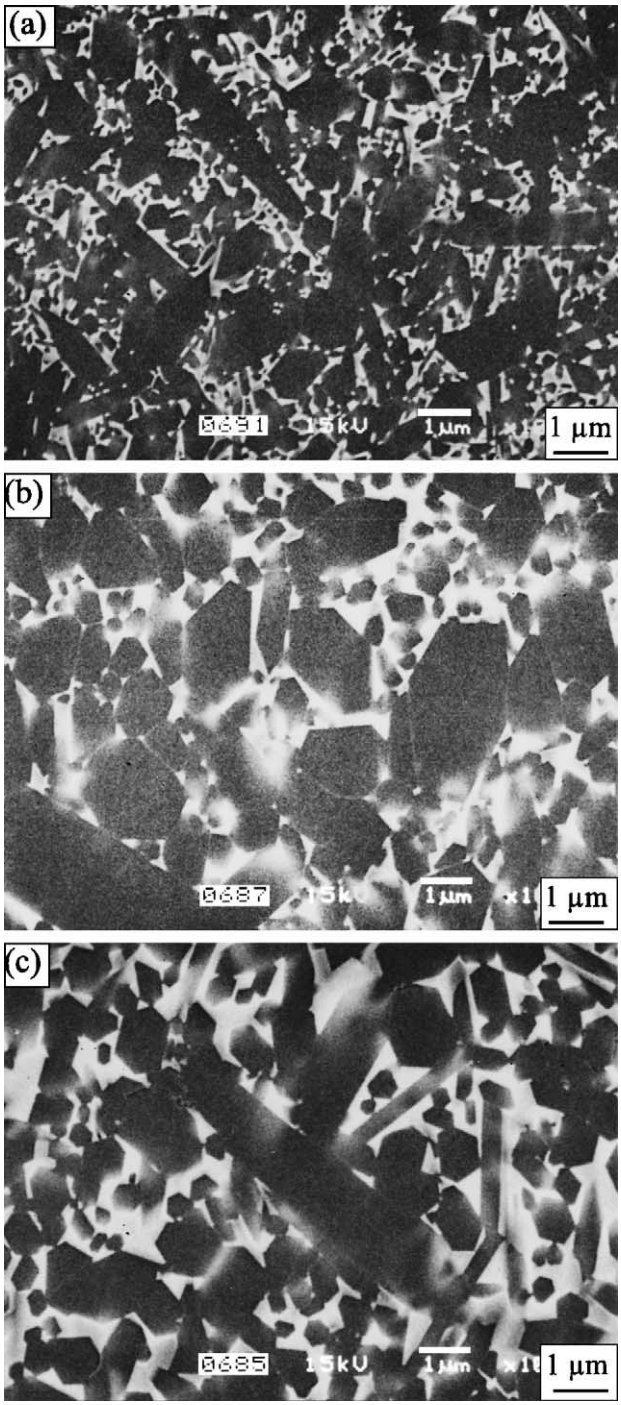

Fig. 1. SEM images of polished and plasma-etched surfaces of microstructures for the hot-pressed Si_3N_4 ceramics with Lu_2O_3 additives; (a) $Lu_2Si_2O_7$–Si_3N_4, (b) $Lu_4Si_2O_7N_2$–Si_3N_4(S), and (c) $Lu_4Si_2O_7N_2$–Si_3N_4(L).

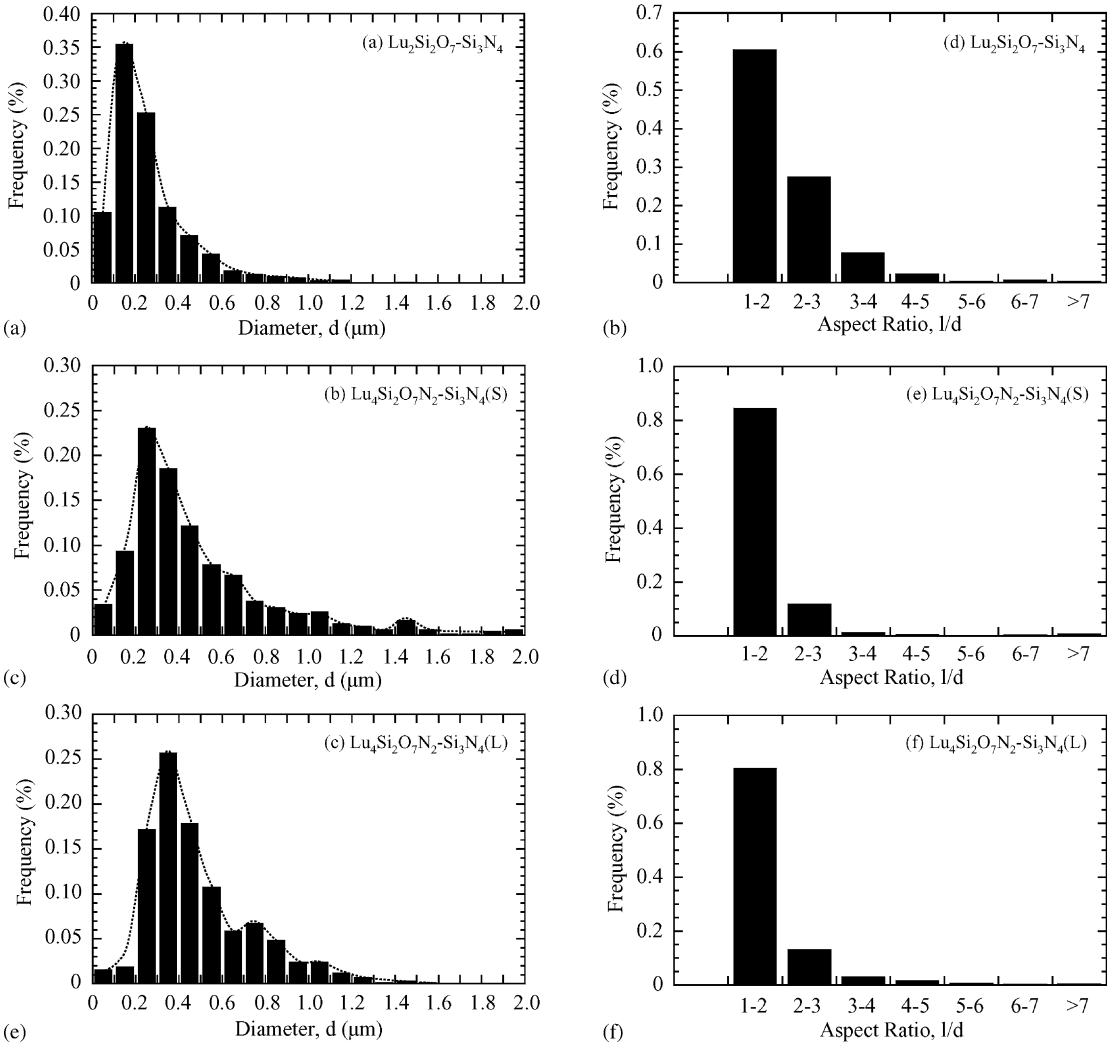

Fig. 2. The histograms of the grain-section diameter and aspect ratio for the hot-pressed Si_3N_4 ceramics with Lu_2O_3 additives; (a) and (d) $Lu_2Si_2O_7$–Si_3N_4, (b) and (e) $Lu_4Si_2O_7N_2$–Si_3N_4(S), and (c) and (f) $Lu_4Si_2O_7N_2$–Si_3N_4(L).

3.2. Fracture toughness

Fracture toughness, K_{IC}, estimated by Vickers indentation crack size measurements for each composition is presented in Table 3. The fracture toughness values for each material vary slightly with increasing applied loads. Typically, for the specimens of coarser grain size ($Lu_4Si_2O_7N_2$–Si_3N_4(S) and $Lu_4Si_2O_7N_2$–Si_3N_4(L)) the

Table 2
Average grain diameter size, aspect ratio and volume fraction of large needle-like grains ($l/d > 4$, $l > 2\,\mu m$) for the hot-pressed Si_3N_4 ceramics with Lu_2O_3 additives

Materials	Average grain diameter d (μm)	Average aspect ratio l/d	vol.% of needle-like grains with $l/d > 4$ and $l > 2$ m
$Lu_2Si_2O_7$–Si_3N_4	0.27	2.1	1.7
$LU_4Si_2O_7N_2$–Si_3N_4(S)	0.48	1.7	2.3
$LU_4Si_2O_7N_2$–Si_3N_4(L)	0.49	1.8	3.3

Table 3
Fracture toughness of the hot-pressed Si_3N_4 ceramics with Lu_2O_3 additives

Material	Indentation load P (N)	Fracture toughness K_{IC} (MPa $m^{1/2}$)
$Lu_2Si_2O_7$–Si_3N_4	98	4.92 ± 0.14
	196	4.67 ± 0.11
	294	4.84 ± 0.13
Average values		4.81 ± 0.13
$Lu_4Si_2O_7N_2$–Si_3N_4(S)	98	5.45 ± 0.15
	196	5.61 ± 0.18
	294	5.82 ± 0.19
Average values		5.63 ± 0.18
$Lu_4Si_2O_7N_2$–Si_3N_4(L)	98	5.98 ± 0.20
	196	6.25 ± 0.21
	294	6.38 ± 0.31
Average values		6.21 ± 0.21

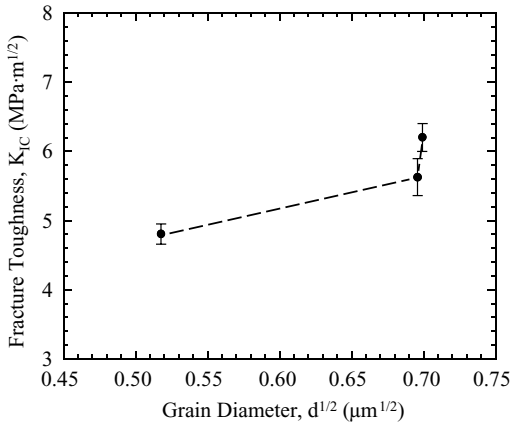

Fig. 3. Plot of the fracture toughness as a function of average grain diameter size, *d*, for the hot-pressed Si_3N_4 ceramics with Lu_2O_3 additives.

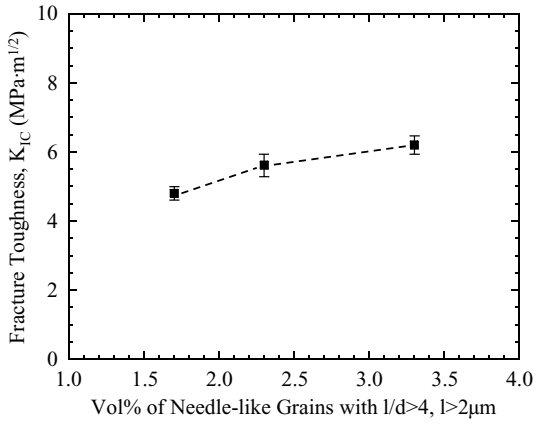

Fig. 4. Plot of the fracture toughness as a function of volume fraction of the large elongated Si_3N_4 grains with aspect ratio $l/d > 4$ and length $l > 2\,\mu m$.

fracture toughness increased with applied load. This suggests that the $Lu_4Si_2O_7N_2$–Si_3N_4(S) and $Lu_4Si_2O_7N_2$–Si_3N_4(L) showed a tendency of higher fracture resistance compared with the $Lu_2Si_2O_7$–Si_3N_4. Among the studied materials, the $Lu_2Si_2O_7$–Si_3N_4 showed the lowest fracture toughness value of 4.81 MPa m$^{1/2}$, and the $Lu_4Si_2O_7N_2$–Si_3N_4(L) had the highest fracture toughness of 6.21 MPa m$^{1/2}$. The fracture toughness of the $Lu_4Si_2O_7N_2$–Si_3N_4(S) was determined to be 5.63 MPa m$^{1/2}$.

Plot of fracture toughness as a function of average grain diameter size is shown in Fig. 3. The fracture toughness increased gradually with increasing the grain diameter size to 0.48 μm and it increased sharply from there once increasing the grain diameter. Furthermore, plot of fracture toughness as a function of the volume fraction of needle-like grains for the three compositions is shown in Fig. 4. It is found that the fracture toughness depends strongly on the volume fraction of needle-like grains. This finding indicated that although the needle-like grains present in the microstructure of the studied materials are not a substantial phase in terms of the volume that they occupy, they dominated the fracture toughness of the materials.

The crack propagation behavior of three compositions was observed under SEM imaging on Vickers indentation cracks in several plasma-etched samples, an example of which is shown in Fig. 5. The predominantly intergranular crack path is observed for the three composition ceramics. This indicates that the crack deflection occurred at the grain boundaries, resulting in the observed Si_3N_4 grain pullout. In addition, the elastic bridging and frictional grains bridging were also observed accompanying with the Si_3N_4 grains pullout. These crack propagation behaviors were observed for each material. This suggests that the similar toughening mechanisms operated in the studied materials.

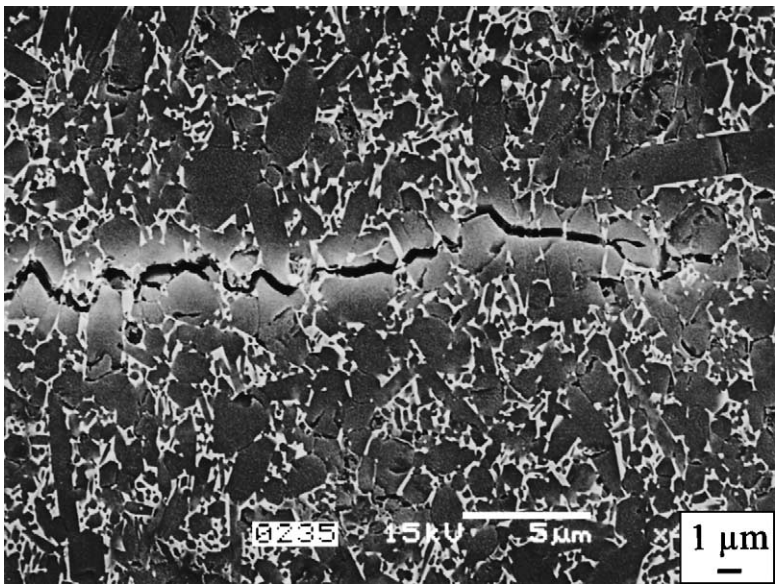

Fig. 5. An example of crack propagation behavior of the hot-pressed Si_3N_4 ceramics with Lu_2O_3 additives ($Lu_4Si_2O_7N_2$–Si_3N_4(S)).

4. Discussion

The distinguishable difference in measured fracture toughness for the three compositions revealed that the fracture toughness was correlated to both the grain-boundary phase composition and amount of additive (Tables 1 and 3), as a result of the different microstructural characterizations, including the grain diameter size, distribution, and morphology (Figs. 1 and 2) [11–14]. On the other hand, SEM observation of crack introduced by a Vickers indentation on the polished surface exhibited nearly the same crack propagation behavior for the studied materials (Fig. 5). This implies that the predominantly fracture toughening mechanism is the same for these materials. However, this mechanism contribution to increasing fracture toughness was different, dependent on the microstructural characterizations. Studies have been reported that the fracture toughness of Si_3N_4 ceramic containing large elongated grains was directly related to the large elongated grains [11–14]. In general, the increases in both the size and volume fraction of elongated grains produced a larger contribution from both frictional bridging and pullout [11–14]. In particular, the presence of needle-like grains (aspect ratio, $l/d > 4$, length, $l > 2\,\mu m$) in ceramic is very effective for increasing fracture toughness [11].

In the present study, the fracture toughness of the $Lu_4Si_2O_7N_2$–Si_3N_4(L), although its average grain diameter size ($d = 0.49\,\mu m$) is nearly the same to that of the $Lu_4Si_2O_7N_2$–Si_3N_4(S) ($d = 0.48\,\mu m$), is significantly larger than that of the $Lu_4Si_2O_7N_2$–Si_3N_4(S) (Tables 2 and 3). This is attributed to the larger volume fraction of the needle-like grains (Fig. 4). This was consistent with the results on fracture toughness for the Si_3N_4 with Y_2O_3–Al_2O_3 additives reported in previous study [11]. Increase in fracture toughness of 30% has been reported for this Si_3N_4, resulting from the presence of approximately 34% of needle-like grains [11]. In addition, it is also found that the increase of fracture toughness caused by the volume fraction of needle-like grains in magnitude was correlated to grain-boundary phase. Fracture toughness of the $Lu_4Si_2O_7N_2$–Si_3N_4(S) increases by ∼17% compared with the $Lu_2Si_2O_7$–Si_3N_4, the corresponding increase in the volume fraction of needle-like grains is ∼35%. On the contrary, although the increase in the volume fraction of needle-like grains in the $Lu_4Si_2O_7N_2$–Si_3N_4(L) is ∼43% compared with the $Lu_4Si_2O_7N_2$–Si_3N_4(S), the corresponding increase in fracture toughness is only ∼10%. This comparison indicated that the increase of fracture toughness was not only dependent on the volume fraction of needle-like grains, but also depended on grain-boundary phase. An early study has been reported that enhancing interfacial debonding between the grains, which was found to be correlated to grain-boundary phase, should result in high fracture toughness [12].

In the studied materials, the triple grain-junction pockets were completely crystallized for the $Lu_2Si_2O_7$–Si_3N_4, whereas these pockets were partially crystallized for the $Lu_4Si_2O_7N_2$–Si_3N_4 [18]. The difference in crystallization behavior suggests that the residual radial tensile stresses produced were larger in the $Lu_2Si_2O_7$–Si_3N_4 than in the $Lu_4Si_2O_7N_2$–Si_3N_4, because the stresses result from a reduction of the volume during the crystallization and from the thermal expansion mismatch between the Si_3N_4 and grain-boundary phase [21]. In addition, the intergranular glass film was thinner for the $Lu_2Si_2O_7$–Si_3N_4 (0.4–0.6 nm) than for the $Lu_4Si_2O_7N_2$–Si_3N_4 (1.0–1.5 nm) [18]. The presence of the amorphous film at two-grain junctions promotes interface debonding [13]. Thus, based on the previous results reported and the knowledge of the interfacial debonding [22,23], it can be concluded that the lower residual internal stresses and thicker glass film promote the interfacial debonding between β-Si_3N_4 grains. This implies that interfacial debonding was enhanced in the $Lu_4Si_2O_7N_2$–Si_3N_4 compared with the $Lu_2Si_2O_7$–Si_3N_4. Therefore, it is reasonable to conclude theoretically that the greater fracture toughness in the $Lu_4Si_2O_7N_2$–Si_3N_4 than the $Lu_2Si_2O_7$–Si_3N_4 results partially from contribution of interfacial debonding although the magnitude of this effect is not well known.

5. Summary

(1) $Lu_2Si_2O_7$–Si_3N_4 showed fine-grained microstructure in which the elongated grains were embedded. The average grain diameter size and aspect ratio were 0.27 μm and 2.1, respectively, and the volume fraction of large needle-like β-Si_3N_4 grains ($l > 2\,\mu m$, $l/d > 4$) was proximately 1.7%.

(2) Microstructures of the $Lu_4Si_2O_7N_2$–Si_3N_4 were found to consist of coarse grains and needle-like grains. The bimodal grain diameter size distribution was observed for the two compositions. Average grain diameter size and aspect ratio were found to be slightly dependent on amount of additive, with $d = 0.48\,\mu m$ and $l/d = 1.7$ for $Lu_4Si_2O_7N_2$– Si_3N_4(S) and $d = 0.49\,\mu m$ and $l/d = 1.8$ for Lu_4Si_2- O_7N_2–Si_3N_4(L). The volume fraction of needle-like β-Si_3N_4 grains ($l > 2\,\mu m$, $l/d > 4$) was greater than that of $Lu_2Si_2O_7$–Si_3N_4 and increased with amount of additive.

(3) Fracture toughness of the $Lu_2Si_2O_7$–Si_3N_4 was determined to be $4.81\,MPa\,m^{1/2}$, and the fracture toughness of the $Lu_4Si_2O_7N_2$–Si_3N_4(S) and $Lu_4Si_2O_7N_2$–Si_3N_4(L) was equal to be 5.63 and $6.21\,MPa\,m^{1/2}$, respectively. This greater fracture toughness for the $Lu_4Si_2O_7N_2$–Si_3N_4 was attributed to large grain size, increase of volume fraction of needle-like grains and enhancing interface debonding, compared to the $Lu_2Si_2O_7$–Si_3N_4. In particular, increase of volume fraction of needle-like grains caused predominantly increase in fracture toughness.

References

[1] W.A. Sanders, D.M. Mieskowski, Strength and microstructure of sintered Si_3N_4 with rare-earth-oxide additions, Am. Ceram. Soc. Bull. 64 (2) (1985) 304–309.

[2] M.K. Cinibulk, G. Thomas, S.M. Johnson, Oxidation behavior of rare-earth disilicate–silicon nitride ceramics, J. Am. Ceram. Soc. 75 (8) (1992) 2044–2049.

[3] M.K. Cinibulk, G. Thomas, S.M. Johnson, Strength and creep behavior of rare-earth disilicate–silicon nitride ceramics, J. Am. Ceram. Soc. 75 (8) (1992) 2050–2055.

[4] H.J. Choi, J.G. Lee, Y.W. Kim, High temperature strength and oxidation behavior of hot-pressed Si_3N_4-disilicate ceramics, J. Mater. Sci. 32 (1997) 1937–1942.

[5] N. Hirosaki, Y. Yamamoto, T. Nishimura, M. Mitomo, Fabrication of Si_3N_4-based ceramics, Japan Patent 324327 (2000).

[6] S.Q. Guo, N. Hirosaki, Y. Yamamoto, T. Nishimura, M. Mitomo, Improvement of high-temperature strength of hot-pressed sintering silicon nitride with Lu_2O_3 addition, Scripta Mater. 45 (2001) 867–874.

[7] J.W. Cao, Y. Takigawa, Y. Yasutomi, Y. Yamamoto, N. Hirosaki, Tensile creep of hot-pressed Si_3N_4 ceramics with Lu_2O_3 additives, in: Annual Meeting of the Ceramic Society of Japan, Osaka, Japan, 24–26 March 2002, p. 50 (in Japanese).

[8] S.Q. Guo, N. Hirosaki, Y. Yamamoto, T. Nishimura, M. Mitomo, Strength retention in hot-pressed silicon nitride ceramics with Lu_2O_3 additives after oxidation exposure in air at 1500 °C, J. Am. Ceram. Soc. 85 (6) (2002) 1607–1609.

[9] G. Ziegler, J. Heinrich, G. Wotting, Relations between processing, microstructure and properties of dense and reaction-bonded silicon nitride, J. Mater. Sci. 22 (1987) 3041–3086.

[10] M. Swain, Structure and Properties of Ceramics, VHC, Weinheim, Germany, 1994.

[11] P. Sajgalik, J. Dusza, M.J. Hoffman, Relationship between microstructure toughening mechanisms and fracture toughness of reinforced silicon nitride ceramics, J. Am. Ceram. Soc. 78 (10) (1995) 2619–2624.

[12] P.F. Becher, E.Y. Sun, K.P. Plucknett, K.B. Alexander, C.H. Hsueh, H.T. Lin, S.B. Waters, C.G. Westmoreland, E.S. Kang, K. Hirao, E. Brito, Microstructural design of silicon nitride with improved fracture toughness. I. Effects of grain shape and size, J. Am. Ceram. Soc. 81 (11) (1998) 2821–2830.

[13] H.-J. Kleebe, G. Pezzotti, G. Ziegler, Microstructure and fracture toughness of Si_3N_4 ceramics: combined roles of grain morphology and secondary phase chemistry, J. Am. Ceram. Soc. 82 (7) (1999) 1857–1867.

[14] B.W. Trice, J.W. Halloran, Mode I fracture toughness of a small-grained silicon nitride: orientation, temperature and crack length effects, J. Am. Ceram. Soc. 82 (10) (1999) 2633–2640.

[15] T. Nishimura, M. Mitomo, Phase relationship in the system Si_3N_4–SiO_2–Yb_2O_3, J. Mater. Res. 10 (2) (1995) 240–242.

[16] O. Yeheskel, O. Tevet, Elastic moduli of transparent yttria, J. Am. Ceram. Soc. 82 (1) (1999) 136–144.

[17] S.Q. Guo, N. Hirosaki, Y. Yamamoto, T. Nishimura, M. Mitomo, Hot-press sintering silicon nitride with Lu_2O_3 addition: elastic moduli and fracture toughness, J. Eur. Ceram. Soc. 23 (2003) 537–545.

[18] S.Q. Guo, N. Hirosaki, Y. Yamamoto, T. Nishimura, H. Tanaka, Effect of grain-boundary phase on flexural strength of hot-pressed Si_3N_4 ceramics with Lu_2O_3 additives, J. Am. Ceram. Soc., submitted for publication.

[19] G.R. Anstis, P. Chantikul, B.R. Lawn, D.B. Marshall, A critical evaluation of indentation techniques for measuring fracture toughness. I. Direct crack measurements, J. Am. Ceram. Soc. 64 (9) (1981) 533–538.

[20] M. Mitomo, S. Uesono, Microstructural development during gas-pressure sintering of α-silicon nitride, J. Am. Ceram. Soc. 75 (1) (1992) 103–108.

[21] W. Pompe, H. Kessler, Internal stresses in silicon nitride and their influence on mechanical behavior, in: M.J. Hoffmann, G. Petzow (Eds.), Tailoring of Mechanical Properties of Si_3N_4 Ceramics, Kluwer Academic Publishers, Netherlands, 1994, p. 353.

[22] S. Prouhet, G. Camus, C. Labrugere, A. Guette, E. Martin, Mechanical characterization of Si-C(O) fiber/SiC (CVI) matrix composites with a BN-interphase, J. Am. Ceram. Soc. 77 (3) (1994) 649–656.

[23] R.N. Singh, S.K. Reddy, Influence of residual stress, interface roughness and fiber coatings on interfacial properties in ceramic composites, J. Am. Ceram. Soc. 79 (1) (1996) 137–147.